Inorganic Chemistry
Article
Cite This: Inorg. Chem. 2018, 57, 326−334
pubs.acs.org/IC

Synthesis, Crystal Structures, and EPR Studies of First $Mn^{III}Ln^{III}$ Hetero-binuclear Complexes

Lívia B. L. Escobar,[†,‡] Guilherme P. Guedes,[§] Stéphane Soriano,[∥] Rafael A. A. Cassaro,[⊥] Jonathan Marbey,[‡] Stephen Hill,*[,‡] Miguel A. Novak,[#] Marius Andruh,*[,▽] and Maria G. F. Vaz*[,†]

[†]Instituto de Química, Universidade Federal Fluminense, Niterói, Rio de Janeiro, 24020-150, Brazil
[‡]Department of Physics and NHMFL, Florida State University, Tallahassee, Florida 32310, United States
[§]Departamento de Química, Instituto de Ciências Exatas, Universidade Federal Rural do Rio de Janeiro, Seropédica, Rio de Janeiro, 23897-970, Brazil
[∥]Instituto de Física, Universidade Federal Fluminense, Niterói, Rio de Janeiro, 24020-140, Brazil
[⊥]Instituto de Química, Universidade Federal do Rio de Janeiro, Rio de Janeiro, 21941-909, Brazil
[#]Instituto de Física, Universidade Federal do Rio de Janeiro, Rio de Janeiro, 21941-972, Brazil
[▽]Inorganic Chemistry Laboratory, Faculty of Chemistry, University of Bucharest, Str. Dumbrava Rosie, no. 23, 020464, Bucharest, Romania

Supporting Information

ABSTRACT: A new family of binuclear complexes $[Mn^{III}Ln^{III}(dpm)_4(MeO)_2(MeOH)_2]$ is reported (where Ln = La^{III} (**1**), Pr^{III} (**2**), and Eu^{III}(**3**)). These compounds were obtained from a one-pot reaction between 2,2,6,6-tetramethyl-3,5-heptanodione (Hdpm), Mn^{II}, and the respective Ln^{III} salt in the presence of sodium methoxide. The derivative containing the diamagnetic ion La^{III} has been synthesized in order to characterize the local anisotropy of the Mn^{III} ion. High-field electron paramagnetic resonance (HFEPR) spectroscopy shows that the Mn^{III} ion, with an elongated octahedral geometry in all compounds, has a significant axial zero-field splitting and a small rhombic anisotropy. Additionally, the HFEPR measurements indicate that there is almost no exchange between the spin carriers in these compounds, all of which exhibit field-induced slow relaxation of the magnetization.

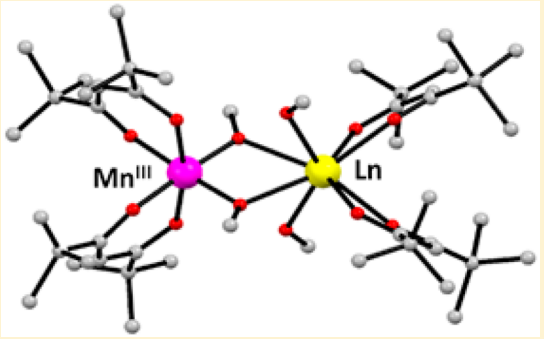

INTRODUCTION

Heterometallic complexes containing 3*d* and 4*f* metal ions are intensively investigated because they may afford hysteretic behavior due to slow relaxation of the magnetization, the so-called Single Molecule Magnets (SMMs), Single Ion Magnets (SIMs, a SMM with only one magnetic ion), and Single Chain Magnets (SCMs).[1−5] The interest in such molecules is justified by their potential applications in high-density information storage and quantum information processing.[6−9] In this context, the selection of metal ions is very important to achieve SMM behavior. Lanthanides are currently employed extensively as ingredient in the synthesis of molecular nanomagnets because of their strong magnetic anisotropy.[10−12]

A large number of heterometallic SMMs have been described to date,[13−15] some of them containing one or more Mn^{III} centers.[16,17] In order to obtain SMMs, the combination of a high-spin Mn^{III} and various lanthanide ions (such as Tb^{III}, Dy^{III}, or Ho^{III}) provides a promising strategy, since all of these ions can show large uniaxial magnetic anisotropy. Thus, the presence of these ions within the same molecular entity may provide sufficient conditions to establish an energy barrier for reversal of magnetic moment.[18−22]

So far, a few Mn^{III}−Ln^{III} SMMs have been reported, with various nuclearities such as Mn_3Ln_4 (Ln = La, Pr, Nd, Gd),[23] Mn_9Dy_8,[24] Mn_6Ln (Ln = La, Dy, Tb),[19] Mn_4Ln_4 (Ln = Sm, Gd, Tb, Dy, Ho, Er, and Y),[25] and Mn_2Ln_2 (Ln = Y, Gd, Tb, Dy, Ho).[26] An interesting study published by Powell and co-workers reported a $Mn_{18}Dy$ cluster in which SMM properties are triggered when Dy^{III} is incorporated into a Mn_{19} complex.[27] However, no binuclear Mn^{III}-Ln^{III} complexes have been reported to date.

Despite the fact that many compounds containing anisotropic first-row transition metals[28] or lanthanides[29,30] with SIM behavior have been reported, only a few examples in which the SIM behavior is attributed to the Mn^{III} ion have been described.[31−33] One of the first examples of a SIM containing the Mn^{III} ion was described by Ishikawa and co-workers, a Mn^{III}-salen-type complex with an energy barrier of 16.5 K.[34]

Received: October 6, 2017
Published: December 19, 2017

DOI: 10.1021/acs.inorgchem.7b02575
Inorg. Chem. 2018, 57, 326−334

Table 1. Summary of the Crystal Structures, Data Collection, and Refinement for 1−3[a]

	1	2	3
chemical formula	$C_{48}H_{90}MnO_{12}La$	$C_{48}H_{90}MnO_{12}Pr$	$C_{48}H_{90}MnO_{12}Eu$
formula mass/g mol^{-1}	1053.06	1055.05	1066.25
crystal system	triclinic	triclinic	triclinic
space group	$P\bar{1}$	$P\bar{1}$	$P\bar{1}$
radiation type	MoKα	MoKα	MoKα
temperature/K	120	140	120
a/Å	10.6514(9)	10.5597(6)	10.5438(9)
b/Å	15.2321(15)	14.9839(9)	14.9019(12)
c/Å	19.808(2)	19.3928(11)	19.3103(15)
α/deg	105.292(4)	104.467(5)	104.595(7)
β/deg	99.497(4)	99.791(5)	99.963(7)
γ/deg	103.526(4)	103.821(5)	103.900(7)
V/Å^3	2924.6(5)	2797.7(3)	2760.7(4)
Z	2	2	2
ρ(calculated), Mg·m^{-3}	1.196	1.252	1.174
μ, mm^{-1}	0.986	1.138	1.403
reflns measured	54387	18711	21253
independent reflns	10684	9872	9738
θ range/deg	2.03−25.37	2.05−25.03	2.05−25.03
index range	$h = -12 \rightarrow 12$	$h = -12 \rightarrow 10$	$h = -12 \rightarrow 10$
	$k = -18 \rightarrow 18$	$k = -12 \rightarrow 10$	$k = -17 \rightarrow 17$
	$l = -23 \rightarrow 23$	$l = -22 \rightarrow 23$	$l = -22 \rightarrow 23$
R_{int}	0.1215	0.0682	0.0730
R_1 values ($I > 2\sigma(I)$)	0.0719	0.0774	0.0625
$wR(F^2)$ values ($I > 2\sigma(I)$)	0.1833	0.1700	0.1420
R_1 values (all data)	0.1203	0.1098	0.0868
$wR(F^2)$ values (all data)	0.2184	0.2023	0.1591
goodness of fit on F^2	1.032	1.065	1.038
CCDC deposition	1496593	1496594	1496596

[a]For (**1**): $w = 1/[\sigma^2(F_o^2) + (0.\ 0.1119P)^2 + 9.1637P]$; for (**2**): $w = 1/[\sigma^2(F_o^2) + (0.0758P)^2 + 15.8104P]$; for (**3**): $w = 1/[\sigma^2(F_o^2) + (0.0633P)^2 + 13.5722P]$, where $P = (F_o^2 + 2F_c^2)/3$.

Prior to our work, just one Mn^{III}-based SIM containing a β-diketonate ligand has been reported in the literature.[35]

In a previous article, we described a useful synthetic route toward $[Mn^{III}{}_2Ln^{III}{}_2]$ (Ln = Gd, Tb, Dy) complexes with SMM behavior.[36] Herein, we report the synthesis, crystal structure, and magnetic properties of three new binuclear systems containing Mn^{III} and a lanthanide ion (La^{III} (**1**), Pr^{III} (**2**), and Eu^{III} (**3**)) obtained using the same methodology reported in the work mentioned above.[36] The derivative containing the La^{III} ion was synthesized in order to characterize the Zero Field Splitting (ZFS) of the Mn^{III} ion energy levels. To the best of our knowledge, we report here the very first HFEPR studies on $Mn^{III}Ln^{III}$ compounds.

EXPERIMENTAL SECTION

Synthesis. All reagents and solvents were purchased from commercial sources and used without further purification.

General Procedure for Compounds 1−3. A 0.220 mmol portion of $Ln(NO_3)_3{\cdot}nH_2O$ (Ln = La, Pr, or Eu), 0.220 mmol of anhydrous $MnCl_2$ (28 mg), and 0.660 mmol of Hdpm (122 mg, 140 μL) were dissolved in 12 mL of methanol. The pale yellow solution was stirred for 5 min, and then, 120 μL of a 30% (m/v) sodium methoxide solution was added and a brown solid was formed. The mixture was stirred for one additional hour and filtered off. The crude product was dissolved in 30 mL of diethyl ether and filtered to remove any insoluble material. Single crystals were obtained after 1−2 days of slow diffusion of methanol into diethyl ether solution. Powder X-ray diffraction patterns for compounds **1**−**3** were compared with the simulated powder diffraction pattern predicted from the crystal structure. The experimental and simulated powder XRD patterns corresponded well in peak positions and relative intensity, confirming the crystalline phase purity of the compounds (see the SI for details, Figure S2).

Compound **1**: Yield: 75%. IR (ν/cm^{-1}): 3327, 2954, 2921, 2865, 1590, 1570, 1500, 1385, 1353, 1285, 1137, 1034 and 1015.

Compound **2**: Yield: 70%. IR (ν/cm^{-1}): 3367, 2965, 2903, 2865, 1592, 1575, 1498, 1388, 1354, 1283, 1137, 1038 and 1010.

Compound **3**: Yield: 73%. IR (ν/cm^{-1}): 3370, 2957, 2902, 2865, 1591, 1571, 1537, 1498, 1458, 1354, 1285, 1225, 1132, 1038 and 1006.

X-ray Diffraction. Powder X-ray diffraction data for all samples were collected on a Bruker D8 Advance equipped with a LynxEye detector at room temperature. Single crystal X-ray diffraction data for compound **1** was collected on a Bruker D8 Venture diffractometer with Mo Kα (λ = 0.71073 Å) radiation at 120 K. Data collection and cell refinement were performed with Bruker Instrument Service v4.2.2 and APEX2,[37] respectively. Data reduction was carried out using SAINT.[38] Empirical multiscan absorption correction using equivalent reflections was performed with the SADABS program.[39] For compounds **2** and **3**, the data were collected on an Oxford GEMINI A Ultra diffractometer with Mo Kα (λ = 0.71073 Å) radiation at low temperature (120 and 140 K, respectively). Data collection, reduction, and cell refinement were performed by CRYSALIS RED, Oxford diffraction Ltd. − Version 1.171.32.38 program.[40] All crystal structures were solved and refined using SHELXS and SHELXL packages.[41] Compounds **1**−**3** presented disorder in the methyl groups, which was modeled considering two possible arrangements. The structures were drawn using the ORTEP-3 for WINDOWS,[42] and VESTA programs.[43] Summaries of the crystal data, data collection, and refinement for compounds **1**−**3** are listed in Table 1. Selected bond lengths and bond

DOI: 10.1021/acs.inorgchem.7b02575
Inorg. Chem. 2018, 57, 326−334

angles are summarized in Table 2. Figure S1 shows the ORTEP representations of the asymmetric units for compounds **1**−**3**.

Table 2. Selected Bond Lengths (Å) and Bond Angles (deg) for 1−3

labels	**1** (Ln = La)	**2** (Ln = Pr)	**3** (Ln = Eu)
Ln1−O1	2.426(6)	2.410(5)	2.362(4)
Ln1−O2	2.440(6)	2.379(5)	2.328(4)
Ln1−O3	2.449(5)	2.382(5)	2.347(4)
Ln1−O4	2.431(5)	2.399(6)	2.348(4)
Ln1−O5	2.619(6)	2.557(6)	2.494(5)
Ln1−O6	2.628(6)	2.570(6)	2.513(5)
Ln1−O7	2.516(5)	2.450(5)	2.409(4)
Ln1−O8	2.499(5)	2.454(5)	2.410(4)
Mn1−O7	1.890(6)	1.889(5)	1.865(4)
Mn1−O8	1.889(5)	1.875(6)	1.871(4)
Mn1−O9	1.943(5)	1.951(5)	1.952(4)
Mn1−O10	2.180(5)	2.180(6)	2.170(5)
Mn1−O11	1.939(5)	1.956(5)	1.953(4)
Mn1−O12	2.189(5)	2.191(6)	2.176(4)
Ln1···Mn1	3.5665(12)	3.4974(13)	3.4450(11)
Ln1−O7−Mn1	107.20(2)	106.63(2)	106.73(19)
Ln1−O8−Mn1	107.79(2)	107.06(2)	106.49(18)
O1−Ln1−O5	82.74(2)	81.92(19)	81.28(16)
O1−Ln1−O7	79.20(2)	79.82(17)	79.30(15)
O5−Ln1−O7	72.16(18)	73.68(19)	74.54(16)
O2−Ln1−O4	80.77(2)	81.1(2)	80.97(16)
O2−Ln1−O6	72.24(2)	70.97(19)	71.31(16)
O4−Ln1−O6	82.77(2)	82.51(19)	81.59(16)
O3−Ln1−O8	121.4(2)	122.59(19)	122.15(16)
O7−Mn1−O8	84.28(2)	84.40(2)	84.16(19)
O7−Mn1−O9	92.51(2)	92.63(2)	93.00(2)
O8−Mn1−O11	92.47(2)	93.15(2)	93.01(19)
O9−Mn1−O11	85.62(2)	89.82(2)	89.80(2)
O7−Mn1−O12	94.71(2)	94.79(2)	95.11(19)
O8−Mn1−O12	93.91(2)	94.10(2)	94.11(19)
O9−Mn1−O12	85.49(2)	86.57(2)	85.43(19)
O11−Mn1−O12	86.65(2)	85.64(2)	86.11(18)
O7−Mn1−O10	93.18(2)	95.30(2)	95.23(19)
O8−Mn1−O10	92.47(2)	93.26(2)	93.20(2)
O9−Mn1−O10	90.76(3)	86.57(2)	87.03(19)
O11−Mn1−O10	86.96(2)	84.55(2)	84.56(19)
O10−Mn1−O12	168.35(2)	168.04(2)	167.87(18)

Magnetization Measurements. DC magnetic measurements were performed on a Cryogenic Sx600 SQUID and/or on a Quantum Design MPMS3 SQUID magnetometer in the temperature range 2−280 K. For compounds **1** and **2**, the samples were placed in a gelatin capsule and the diamagnetic data were corrected for the contribution of the sample and holder. Crystals of **3** were first wrapped in polytetrafluoroethylene tape and pressed into a pellet. The sample's diamagnetism correction was estimated from Pascal's constants. AC magnetic measurements were performed on a Quantum Design PPMS system using the same samples.

EPR Spectroscopy. High-field, high-frequency EPR measurements were carried out at the U.S. National High Magnetic Field Laboratory (NHMFL), in Tallahassee, Florida, on powder samples of compounds **1**−**3** and on a single crystal of **1**.

The powder spectra were recorded at temperatures ranging from ca. 4 K to 30 K on a home-built spectrometer at the EMR facility of the NHMFL.[44] The instrument is a transmission-type device in which microwaves are propagated in cylindrical lightpipes. The microwaves are generated by a phase-locked Virginia Diodes source generating frequencies in the range from 101.6 to 628.8 GHz. A superconducting magnet (Oxford Instruments) capable of reaching a field of 17 T was employed. The pure powder samples obtained by grinding the single crystals were constrained to prevent magnetic torquing at high magnetic fields. All simulations of powder EPR spectra were performed using the EasySpin software.[45]

Single crystal measurements were performed in a 7 T horizontal-bore, split-gap superconducting magnet with temperature control achieved using a ^{4}He flow cryostat. A Millimeter-wave Vector Network Analyzer served as the microwave source and detector via two phase-locked YIG sources.[46,47] Cavity perturbation was employed to measure a very small, needle-shaped single crystal with approximate dimensions of 0.582 × 0.208 × 0.204 mm.

RESULTS AND DISCUSSION

The three complexes were obtained by a one-pot reaction, in which $MnCl_2$ and $Ln(NO_3)_3$ reacted with 2,2,6,6-tetramethyl-3,5-heptanodione (Hdpm) with the further addition of a 30% (m/v) sodium methoxide solution. In these syntheses, the Mn^{II} ions are oxidized *in situ* to Mn^{III}. It is well-known that the presence of electron donating groups attached to the *β*-diketonate ligand, like *tert*-butyl groups in Hdpm, plays an important role in the Mn^{II}-to-Mn^{III} oxidation rate when opened to air.[48]

The radius of the lanthanide (r_{Ln}) ions plays a significant role in the properties and nuclearities of the complexes. Rinck and co-workers investigated the influence of the Ln radius on the nuclearities of complexes with an N-substituted diethanolamine ligand. They observed that smaller lanthanide ionic radii lead to complexes with low nuclearity,[49] in contrast to this work. Recently, some of us described three tetranuclear $[Mn^{III}_2Ln^{III}_2]$ (Ln = Gd, Dy, and Tb) compounds obtained using the same synthetic procedure[36] reported herein. Thus, in the synthesis of heteronuclear compounds containing Mn^{III} and Ln^{III} ions, we observed that the use of lanthanide ions with small ionic radii leads to coordination compounds with high nuclearity, while those from the beginning of the lanthanide series afforded binuclear species.

Description of the Structures. Compounds **1**−**3** are isostructural consisting of neutral hetero-binuclear $[Mn^{III}Ln^{III}(dpm)_4(OMe)_2(MeOH)_2]$ species (Figure 1). The Mn^{III} ion

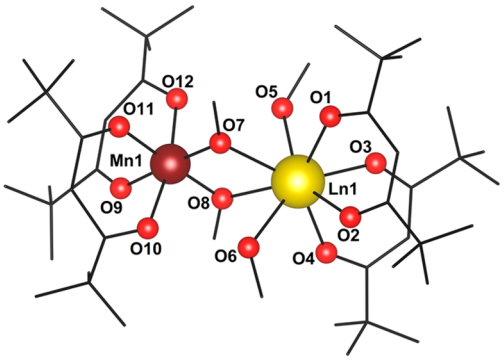

Figure 1. Structure of compounds **1**−**3**. Hydrogen atoms have been omitted for the sake of clarity.

sits in a distorted octahedral environment, being *cis*-coordinated by two μ_2-methoxido oxygen atoms (O7 and O8) and four oxygen atoms (O9, O10, O11, and O12) from two bidentate dpm ligands. Because of the Jahn−Teller distortion expected for the high spin d^4 configuration, the Mn^{III} ion shows an elongated octahedral geometry, with the longer bond lengths as follows: [for **1**, Mn1−O10 = 2.181(6) Å and Mn1−O12 =

DOI: 10.1021/acs.inorgchem.7b02575
Inorg. Chem. 2018, 57, 326−334

2.189(6) Å; for **2**, Mn1−O10 = 2.180(6) Å and Mn1−O12 = 2.191(6) Å; for **3**, Mn1−O10 = 2.171(5) Å and Mn1−O12 = 2.176(4) Å]. The Mn^{III} and Ln^{III} ions are bridged by the oxygen atoms from the two methoxido groups, leading to a heterobinuclear species.

The Ln^{III} ion has a coordination number of eight, being coordinated by four oxygen atoms (O1, O2, O3, and O4) from two dpm ligands, and four oxygen atoms (O5, O6, O7, and O8) from two methanol, and two μ_2-methoxido, respectively. The coordination geometry of the lanthanide(III) ions was calculated using Shape software.[50] It is better described as a biaugmented trigonal prism (Figure 2), but very close to the

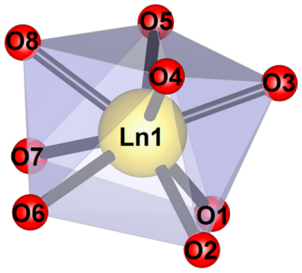

Figure 2. Coordination environment of the lanthanide ion in compounds **1**−**3**.

Snub diphenoid geometry (see Table S1, Supporting Information). The bond lengths between the Ln^{III} ion and the oxygen atoms are in the ranges of 2.354(3)−2.426(6) Å for O1, 2.328(4)−2.440(6) Å for O2, 2.344(3)−2.449(6) Å for O3, 2.348(4)−2.431(6) Å for O4, 2.494(5)−2.619(6) Å for O5, 2.513(5)−2.628(6) Å for O6, 2.409(4)−2.516(5) Å for O7, 2.410(4)−2.499(5) Å for O8. These bond lengths are in the range found in the literature for other Ln-based complexes.[51,52]

The intramolecular distances between Mn^{III} and Ln^{III} are 3.566(1) Å in **1**, 3.497(13) Å in **2**, and 3.445(11) Å in **3**. The shortest intermolecular distances between two metal ions are approximately 8.60, 9.20, and 11.38 Å for $Mn^{III}\cdots Mn^{III}$, $Mn^{III}\cdots Ln^{III}$, and $Ln^{III}\cdots Ln^{III}$, respectively, for all compounds. Intramolecular hydrogen bonding between the hydrogen atom of the hydroxyl group (Donor) from methanol and the adjacent β-diketonate oxygen atom (Acceptor) is established in compounds **1**−**3**, with distances between the donor (O5 and O6) and acceptor (O10 and O12) atoms of 2.868(6) and 2.864(7) Å for **1**, 2.854(7) and 2.822(7) Å for **2**, 2.828(6) and 2.801(6) Å for **3**, respectively, while the D−H···A angles are 139.7(4)° and 142.2(4)° for **1**, 130.0(4)° and 140.1(4)° for **2**, and 139.3(4)° and 126.4(3)° for **3**, respectively.

Magnetic Properties. The magnetic susceptibilities were investigated using a SQUID magnetometer in the 2−240 K temperature range for compound **1** and 2−280 K for compounds **2** and **3**. Plots of $\chi_M T$ versus T, where χ_M is the molar magnetic susceptibility, are shown in Figure 3. The $\chi_M T$ values at the highest temperatures are 3.0 (**1**), 4.6 (**2**), and 4.3 (**3**) $cm^3\ mol^{-1}\ K$. These values correspond to the expected ones for uncoupled Mn^{III} and Ln^{III} spins for compounds **1**−**2**, by considering La^{III} (nonmagnetic), Mn^{III} [^5E_g, i.e., $S = 2$, $g = 2.00$, $(\chi_M T)_{para} = 3.0\ cm^3\ mol^{-1}\ K$], and Pr^{III} [$^3H_4$, i.e., $S = 1$, $L = 5$, $J = 4$, $g_J = 4/5$, $(\chi_M T)_{para} = 1.6\ cm^3\ mol^{-1}\ K$]. For complex **3**, since the first excited spin−orbit coupled state of the Eu^{III} ($^7F_1$) ion lies relatively close in energy (ca. 350 cm^{-1}) to its ground state ($^7F_0$), it can be significantly populated at room

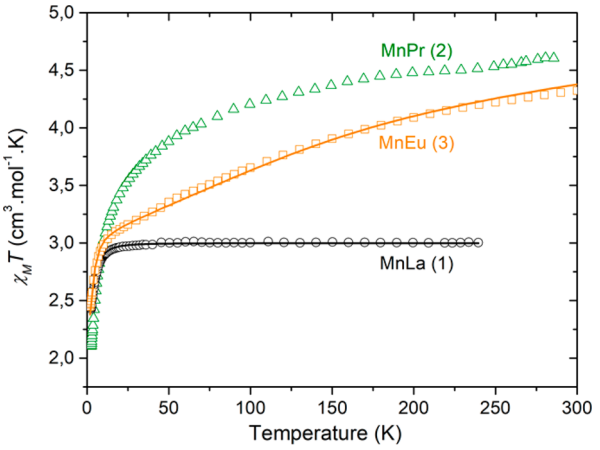

Figure 3. Thermal dependences of the $\chi_M T$ product at 1 kOe for **1**−**3**. The solid lines correspond to the best fits for **1** and **3** (vide text).

temperature. As a consequence, the high temperature value of $\chi_M T$ for **3** is higher than the expected one (3.0 $cm^3\ mol^{-1}K$).[53,54]

For **1**, upon lowering the temperature to 30 K, $\chi_M T$ remains approximately constant and then decreases down to 2.2 $cm^3\ mol^{-1}\ K$ at 1.8 K. Since the La^{III} ion is diamagnetic, the decrease of $\chi_M T$ comes from the depopulation of magnetic sublevels of the Mn^{III} ion due to its zero-field splitting (ZFS) (Figure 3). In order to reproduce the magnetic behavior of compound **1**, the following Hamiltonian was considered:

$$\hat{H} = g\mu_B \vec{B}\cdot\hat{S} + D\hat{S}_z^2 + E(\hat{S}_x^2 - \hat{S}_y^2) \quad (1)$$

The first term represents the Zeeman interaction, while the last two define the second-order ZFS terms. Since the fitting results showed very small dependence on E, this parameter was fixed to zero. The solid line in Figure 3 shows the best fit obtained with $g = 2.00$, and $D_{Mn} = -2.80\ cm^{-1}$ using the MagProp routine in the DAVE software suite.[55] These parameters lie within the range found in the literature for other mononuclear Mn^{III} complexes.[35]

For compounds **2**−**3**, the $\chi_M T$ values decrease continuously as the temperature is lowered. Since the EPR data indicate that there is almost no exchange between the metal ions in these compounds (see below), their magnetic behavior results from the sum of the individual contributions of the Mn^{III} ion and the lanthanide ion. For the praseodymium derivative, its magnetic contribution is due to the depopulation of Stark sublevels,[56] and in the absence of further information on the crystal field, we made no attempt to fit the $\chi_M T$ vs T data. In contrast, for the europium derivative, its magnetic behavior comes primarily from the depopulation of the low-lying spin−orbit coupled state.[54] Therefore, the magnetic behavior of compound **3** was analyzed considering independently the axial ZFS term of the Mn^{III} ion and the spin−orbit coupling of the lanthanide ion (vide the SI).[53,54,57] The yellow solid line in Figure 3 shows the best fit found with $g = 2.01$, $D_{Mn} = -2.4\ cm^{-1}$, and $\lambda = 345\ cm^{-1}$. These parameters are consistent with those of other complexes found in the literature.[35,53,54,57,58] In addition, the very good fitting curves corroborate the EPR conclusion that almost no exchange is effective between the spin carriers. Meanwhile, for all compounds, the magnetization versus H/T curves at 1.8 and 4.0 K do not overlap, indicating significant magnetic anisotropy (Figure S3). For compound **1** in

DOI: 10.1021/acs.inorgchem.7b02575
Inorg. Chem. 2018, 57, 326−334

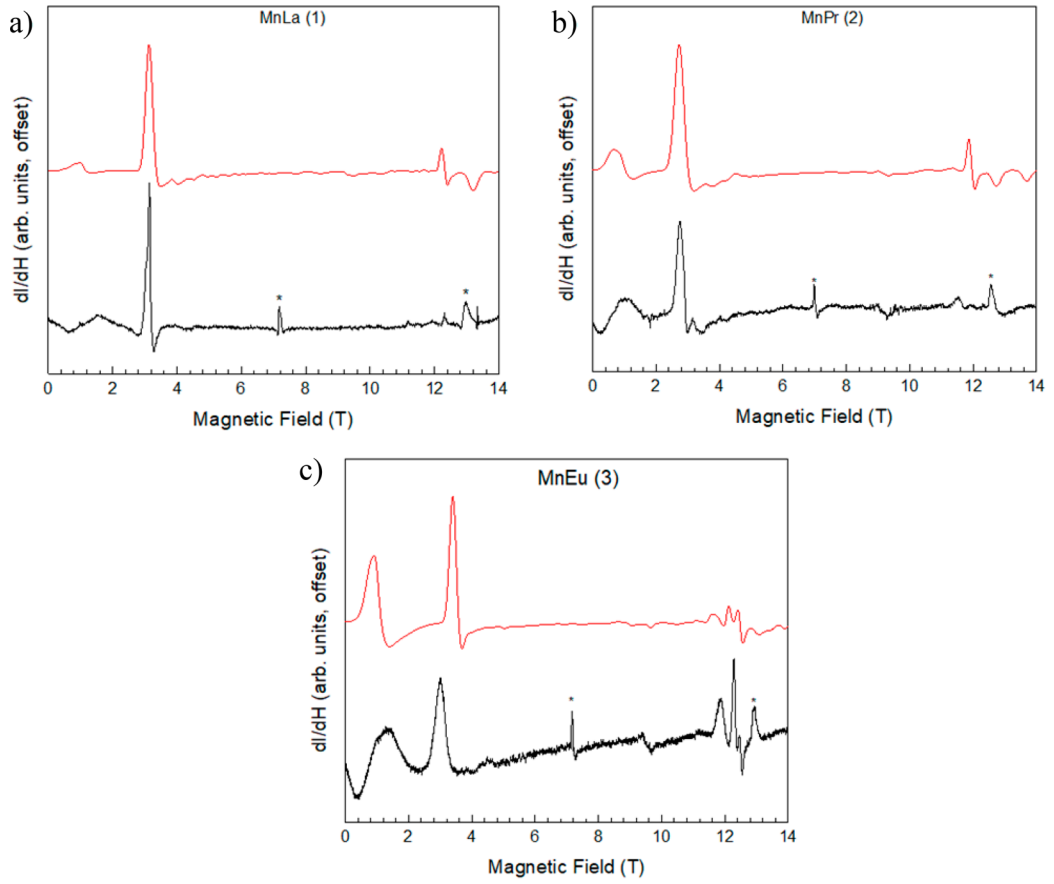

Figure 4. High-field EPR spectra (in black) recorded in derivative mode at 419 GHz and 6 K for **1** (a) and **3** (c), and 409 GHz for **2** (b). It is apparent that two Mn^{III} species with slightly different ZFS parameters contribute to these spectra. To reflect this, the spectra simulated according to the parameters shown in Table 3 were appropriately weighted and summed (in red), as shown above the experimental spectra. The features marked by (∗) are due to surface adsorbed molecular oxygen. Details regarding the simulations are addressed in Figure S6.

Table 3. ZFS Parameters for the Two Species of Compounds 1−3, Including the Relative Weights Needed To Best Simulate the Powder EPR Spectra

	species **1**				species **2**			
	D (cm^{-1})	E (cm^{-1})	weight (%)	line width (mT)	D (cm^{-1})	E (cm^{-1})	weight (%)	line width (mT)
MnLa (**1**)	−3.7	0.1	95	120	−4.6	0.4	5	200
MnPr (**2**)	−3.7	0.1	85	130	−4.6	0.5	15	180
MnEu (**3**)	−3.7	0.1	70	120	−4.6	0.5	30	200

particular, it is noteworthy that the Hamiltonian described in eq 1 reproduces the experimental curve well (Figure S3).

In order to directly determine the ZFS parameters for the Mn^{III} ion, EPR was performed on powders of **1**−**3**. Representative spectra at 419 GHz for **1** and **3** and 409 GHz for **2** are displayed in Figure 4. In these compounds, the Jahn−Teller distortion of the Mn^{III} ion yields a tetragonally elongated octahedral coordination environment, which shows significant deviation from idealized O_h symmetry. The strong resonance close to zero field in Figure 4 gives an approximate measure of the magnitude of the ZFS resulting from this distortion. The temperature dependence (Figure S5) demonstrates that the relative EPR intensities change markedly upon warming/cooling, from which the sign of D can be determined to be negative. The doubling of some of the peaks at high fields indicates the presence of a small rhombicity in the ZFS, represented by E.

Analysis of the recorded EPR spectra shows that they can be entirely simulated by considering only contributions from the Mn^{III} ion for each compound. This result is fully expected for compound **1**, where the La^{III} is diamagnetic, as well as for compound **3**, in which only the nonmagnetic spin−orbit coupled ground state ($^7F_0$) of the Eu^{III} ion is populated at temperatures below 30 K. Interestingly, this is also true for compound **2**, indicating that the Pr^{III} ion is EPR-silent at the frequencies utilized. This observation might be associated with the fact that lanthanide ions can exhibit large ZFS due to their high magnetic anisotropy. Moreover, this indicates that any magnetic interaction between the Mn^{III} and Pr^{III} ion is very weak and can be neglected in the simulations of the EPR spectra. Indeed, the contracted nature of the *4f*-orbitals makes exchange coupling of these paramagnetic centers difficult.

Spectral simulations of the powder EPR measurements were performed by considering the Hamiltonian described by eq 1. Though the spectra can largely be recreated by considering a

DOI: 10.1021/acs.inorgchem.7b02575
Inorg. Chem. 2018, 57, 326−334

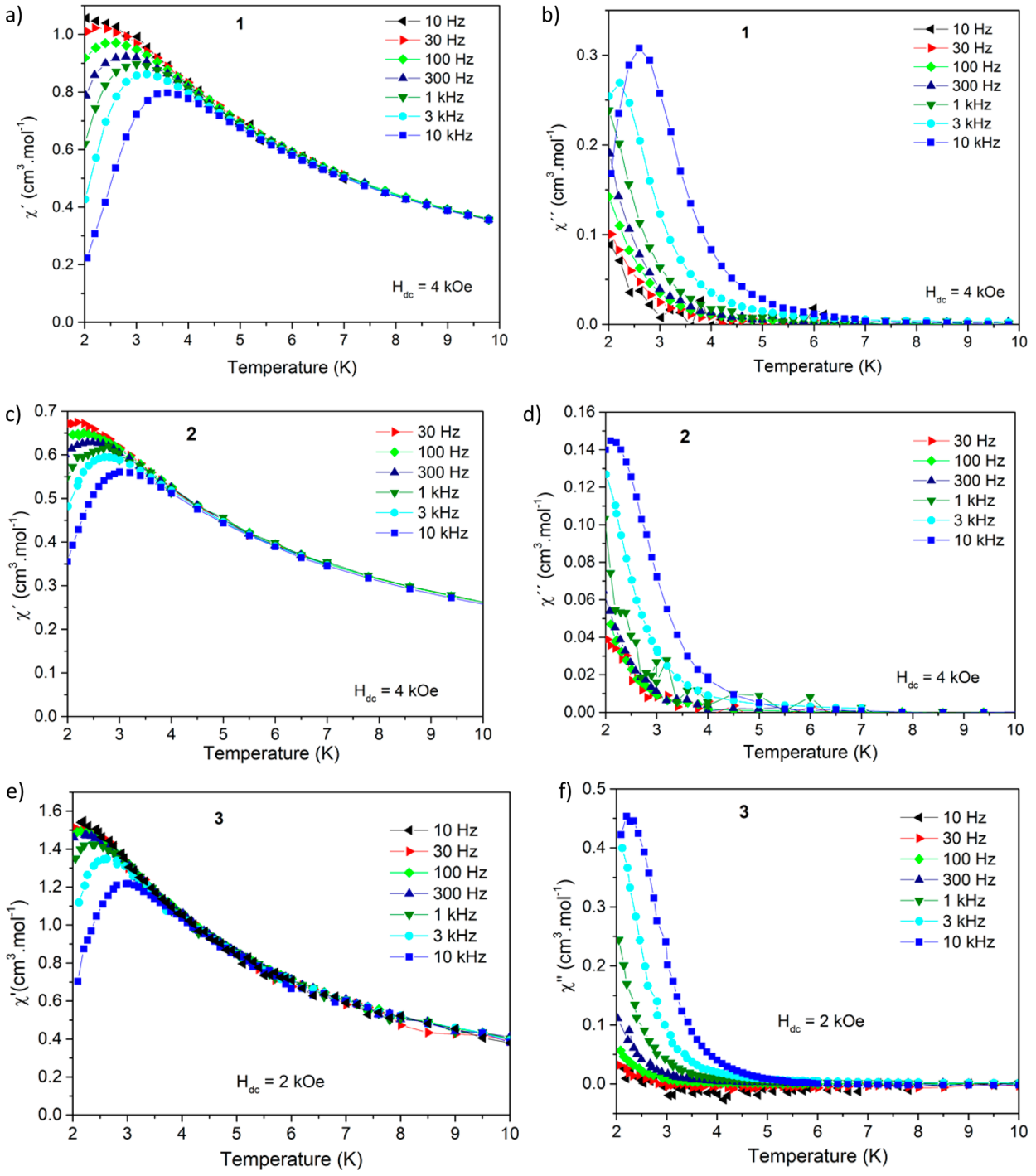

Figure 5. ac susceptibility data between 10 Hz and 10 kHz, from 2 to 10 K, for compounds **1**–**3**: (a, c, e) in-phase (χ'), and (b, d, f) out-of-phase (χ''), components under a static magnetic field.

single species of Mn^{III} (species 1), it was found that another Mn^{III} species (species 2) was present in all three compounds. The presence of these two species could be related to the passage of some insoluble product in the filtration step after the synthesis of the compounds. As such, some impurities not noticeable by the eye could be attached to the single crystals that were manually separated and ground for the acquisition of powder EPR spectra. The relative weights of species **1** and **2** used in the simulations are shown in Table 3.

Spectral simulations were therefore built up from the two Mn^{III} species with different ZFS parameters. These simulations were performed using EasySpin and are included above the experimental spectra in Figure 4 (black = data, red = simulations); details regarding the summation of the simulations for the two species can be found in Figure S6. The best simulated EPR spectra were obtained assuming an isotropic g = 2.00 for both Mn^{III} species and the ZFS parameters summarized in Table 3. These parameters are in the range observed for other Mn^{III}-based complexes reported in the literature.[33,34,58,59]

To confirm the parametrization obtained from the powder data, multifrequency measurements were performed on a

DOI: 10.1021/acs.inorgchem.7b02575
Inorg. Chem. 2018, 57, 326−334

crystal of **1**. An overmoded cavity was employed, enabling fine-frequency steps in the vicinity of the expected zero-field gap between the ground and first excited states of the Mn^{III} ion. Crystal rotation was also employed in order to achieve approximate alignment between the externally applied magnetic field and the easy axis of the Mn^{III} ZFS tensor. Figure S7 shows frequency-dependent spectra (95−367 GHz) recorded at 4 K. Meanwhile, temperature-dependent measurements (4−20 K, not shown) indicate that the transitions observed at low fields in the 280−370 GHz frequency range correspond to excitations from the $m_S = \pm 2$ ground states, thus confirming the negative sign of the D parameter. Extrapolation of these transitions to zero field suggests a gap of 330 ± 10 GHz between the $m_S = \pm 2$ and ±1 quasi-doublets, corresponding to an axial ZFS parameter $D = -3.7$ cm^{-1}, based on the parametrization of eq 1. This value agrees very well with the one used to simulate the dominant signal (Species 1) in the powder spectra. No evidence for a signal from Species 2 could be detected from the crystal measurements, suggesting that the sample employed for these measurements was pure. Further details regarding the analysis of the crystal measurements are given in the SI.

Given the significant easy-axis-type anisotropy associated with the Mn^{III} ion, as evidenced by the static magnetic properties and EPR results, the dynamic magnetic properties of compounds **1**−**3** were investigated by temperature- and frequency-dependent ac magnetic susceptibility measurements. No clear frequency dependence was seen in the in-phase or out-of-phase components under zero static magnetic field. This must occur due to the quantum tunneling of the magnetization (QTM) allowed by the small rhombic E component. However, it is well-known that QTM occurring at zero field, which may be particularly fast in the case of SIMs, can be inhibited via a nonzero externally applied field, removing the quasi-degeneracy of the ground states, and resulting in slow frequency-dependent magnetization dynamics.

Therefore, the ac susceptibilities were measured under static magnetic fields of 4 kOe (**1** and **2**) and 2 kOe (**3**), and all compounds exhibited frequency-dependent maxima in both the in-phase (χ') and out-of-phase (χ'') susceptibilities (Figure 5). These observations represent a clear signature of the presence of slow relaxation of the magnetization. In order to obtain the relaxation times, the frequency dependence of isothermal ac susceptibility at different temperatures (Figure S8) were fitted to a Debye model.[60,61] For all compounds, the relaxation times could be fitted to Arrhenius plots (Figure S9) giving energy barriers of $\Delta E/k_B = 15.0 \pm 0.5$, 8.2 ± 2.0, and 13.0 ± 0.4 K, and pre-exponential factors of $\tau_0 = (4.0 \pm 0.9) \times 10^{-8}$, $(4.1 \pm 1.0) \times 10^{-7}$, and $(3.6 \pm 0.7) \times 10^{-8}$ s for compounds **1**, **2**, and **3**, respectively. These values are consistent with SIM behavior, and close to the values reported for mononuclear Mn^{III}-based complexes by Craig and co-workers (14 K and 6.4×10^{-6} s),[32] and by Pascual-Ávarez and co-workers (22 K and 2.0×10^{-8} s).[33] The difference of the applied magnetic field during the measurements for compounds **1** and **3** could explain the small difference observed in the respective energy barriers.[32,33] In lanthanide-based complexes, magnetic interaction (exchange or dipolar), even small, can affect the relaxation mechanism.[21] This could explain the lower energy barrier of **2**, even if no appreciable coupling could be inferred from EPR measurements.

Given the fact that the Ln^{III} ion is diamagnetic in two of the cases (**1** and **3**) and that the ac response is quite similar in all compounds, it is clear that the slow relaxation must be dominated by the anisotropic Mn^{III} site within each molecule. Moreover, given the absence of any evidence for an appreciable coupling between the Mn^{III} and Pr^{III} ion in compound **2**, the ac response suggests strongly a field-induced SIM behavior associated with the Mn^{III} in all cases.

CONCLUSIONS

We have reported the first examples of $Mn^{III}Ln^{III}$ binuclear complexes. The magnetic properties of all compounds come down to the individual contributions of the constituent magnetic ions, suggesting only weak magnetic coupling between the Mn^{III} and Ln^{III} components. In all complexes, the Mn^{III} ion exhibits a tetragonal elongation of the axial donor atoms (D_{4h} symmetry), which has been proven to result in a negative axial ZFS ($D \sim -3.7$ cm^{-1}), as confirmed by using magnetization measurements and HFEPR spectroscopy. The dynamic magnetic properties, under a static magnetic field, revealed that all compounds exhibit slow relaxation of the magnetization, attributed to the Mn^{III} ion.

ASSOCIATED CONTENT

Supporting Information

The Supporting Information is available free of charge on the ACS Publications website at DOI: 10.1021/acs.inorgchem.7b02575.

The ORTEP representation of the asymmetric units of compounds **1**−**3** (Figure S1). Experimental and simulated powder X-ray diffraction (PXRD) (Figure S2). The isothermal magnetization M versus H/T curves measured at 1.8 and 4 K for compounds **1**−**3** (Figure S3). The Zeeman energy level diagram, the temperature-dependent powder EPR spectra, details about the spectral simulations of the powder EPR spectra for all compounds, and the frequency-dependent HFEPR spectra recorded on a crystal of **1** (Figures S4−S7). Out-phase component (χ'') versus frequency and Arrhenius plot (Figures S8 and S9) (PDF)

Accession Codes

CCDC 1496593, 1496594, and 1496596 contain the supplementary crystallographic data for this paper. These data can be obtained free of charge via www.ccdc.cam.ac.uk/data_request/cif, or by emailing data_request@ccdc.cam.ac.uk, or by contacting The Cambridge Crystallographic Data Centre, 12 Union Road, Cambridge CB2 1EZ, UK; fax: +44 1223 336033.

AUTHOR INFORMATION

Corresponding Authors

*E-mail: mariavaz@vm.uff.br (M.G.F.V.).
*E-mail: marius.andruh@dnt.ro (M.A.).
*E-mail: shill@magnet.fsu.edu (S.H.).

ORCID

Guilherme P. Guedes: 0000-0001-6138-9943
Marius Andruh: 0000-0001-8224-4866
Maria G. F. Vaz: 0000-0001-9855-5909

Notes

The authors declare no competing financial interest.

ACKNOWLEDGMENTS

The authors are thankful for the financial support provided by the Brazilian agencies FAPERJ, and CNPq. We also acknowl-

DOI: 10.1021/acs.inorgchem.7b02575
Inorg. Chem. 2018, 57, 326−334

edge LabCri-UFMG (Brazil), and LDRX-UFF (Brazil) for use of their laboratory facilities. L.B.L.E. acknowledges CAPES for the fellowship that allowed part of this work to be performed at the NHMFL-USA. S.H. acknowledges the support of the U.S. National Science Foundation (DMR-1610226). Work performed at the NHMFL is supported by the NSF (DMR-1157490) and the State of Florida. S.S. thanks the Brazilian Conselho Nacional de Desenvolvimento Cientifico e Tecnológico (CNPq). The authors acknowledge UFSCAR supported by FAPESP 09/54082-2 for the magnetic measurements.

REFERENCES

(1) Andruh, M.; Costes, J. P.; Diaz, C.; Gao, S. 3d-4f Combined Chemistry: Synthetic Strategies and Magnetic Properties. *Inorg. Chem.* **2009**, *48*, 3342−3359.
(2) Polyzou, C. D.; Efthymiou, C. G.; Escuer, A.; Cunha-Silva, L.; Papatriantafyllopoulou, C.; Perlepes, S. P. In search for 3d/4f-metal single-molecule magnets: Nickel(II)/lanthanide(III) coordination clusters. *Pure Appl. Chem.* **2013**, *85*, 315−324.
(3) Feltham, H. L. C.; Brooker, S. Review of purely 4f and mixed-metal nd-4f single-molecule magnets containing only one lanthanide ion. *Coord. Chem. Rev.* **2014**, *276*, 1−33.
(4) Sharples, J. W.; Collison, D. The coordination chemistry and magnetism of some 3d-4f and 4f amino-polyalcohol compounds. *Coord. Chem. Rev.* **2014**, *260*, 1−20.
(5) Sessoli, R.; Powell, A. K. Strategies towards single molecule magnets based on lanthanide ions. *Coord. Chem. Rev.* **2009**, *253*, 2328−2341.
(6) Liu, J. L.; Wu, J. Y.; Chen, Y. C.; Mereacre, V.; Powell, A. K.; Ungur, L.; Chibotaru, L. F.; Chen, X. M.; Tong, M. L. A Heterometallic Fe^{II}−Dy^{III} Single-Molecule Magnet with a Record Anisotropy Barrier. *Angew. Chem., Int. Ed.* **2014**, *53*, 12966−12970.
(7) Shiddiq, M.; Komijani, D.; Duan, Y.; Gaita-Ariño, A.; Coronado, E.; Hill, S. Enhancing coherence in molecular spin qubits via atomic clock transitions. *Nature* **2016**, *531*, 348−351.
(8) Timco, G. A.; Carretta, S.; Troiani, F.; Tuna, F.; Pritchard, R. J.; Muryn, C. A.; McInnes, E. J. L.; Ghirri, A.; Candini, A.; Santini, P.; Amoretti, G.; Affronte, M.; Winpenny, R. E. P. *Nat. Nanotechnol.* **2009**, *4*, 173.
(9) Biswas, S.; Bag, P.; Das, S.; Kundu, S.; van Leusen, J.; Kogerler, P.; Chandrasekhar, V. Heterometallic $[Cu_2Ln_3]$ (Ln = Dy^{III}, Gd^{III} and Ho^{III}) and $[Cu_4Ln_2]$ (Ln = Dy^{III}, and Ho^{III}) Compounds: Synthesis, Structure, and Magnetism. *Eur. J. Inorg. Chem.* **2017**, 1129−1142.
(10) Liu, M.-J.; Hu, K.-Q.; Liu, C.-M.; Cui, A.-L.; Kou, H.-Z. Metallocyclic $Ni_4Ln_2M_2$ single-molecule magnets. *Dalton Trans.* **2017**, *46*, 6544−6552.
(11) Han, H.; Li, X.; Zhu, X.; Zhang, G.; Wang, S.; Hang, X.; Tang, J.; Liao, W. Single-Molecule-Magnet Behavior in a Calix[8]arene-Capped $\{Tb_6^{III}Cr^{III}\}$ Cluster. *Eur. J. Inorg. Chem.* **2017**, 2088−2093.
(12) Reis, S. G.; Briganti, M.; Martins, D. O. T. A.; Akpinar, H.; Calancea, S.; Guedes, G. P.; Soriano, S.; Andruh, M.; Cassaro, R. A. A.; Lahti, P. M.; Totti, F.; Vaz, M. G. F. First coordination compounds based on a bis-(imino nitroxide) biradical and 4*f* metal ions: synthesis, crystal structures and magnetic properties. *Dalton Trans.* **2016**, *45*, 2936−2944.
(13) Zhang, S.; Li, H.; Duan, E.; Han, Z.; Li, L.; Tang, J.; Shi, W.; Cheng, P. A 3D Heterometallic Coordination Polymer Constructed by Trimeric {NiDy2} Single-Molecule Magnet Units. *Inorg. Chem.* **2016**, *55*, 1202−1207.
(14) Xiang, H.; Lu, W.-G.; Jiang, L.; Zhang, W.-X.; Lan, Y. A Family of Double Cubanes $\{Cr^{III}_2Ln^{III}_4O_6\}$ (Ln = Tb, Ho, Er, Yb, Y) Based on Sulfate: Single-Molecule Magnet Behavior in the Terbium and Erbium Analogues. *Eur. J. Inorg. Chem.* **2016**, *2016*, 907−912.
(15) Kajiwara, T.; Nakano, M.; Takahashi, K.; Takaishi, S.; Yamashita, M. Structural Design of Easy-Axis Magnetic Anisotropy and Determination of Anisotropic Parameters of $Ln^{III}Cu^{II}$ Single-Molecule Magnets. *Chem. - Eur. J.* **2011**, *17*, 196−205.
(16) Abeywardana, C.; Mowson, A. M.; Christou, G.; Takahashi, S. Spin coherence in a Mn3 single-molecule magnet. *Appl. Phys. Lett.* **2016**, *108*, 042401.
(17) Sun, L.; Chen, H.; Ma, C.; Chen, C. A new topology of hexanuclear $[Mn^{III}_4Ln^{III}_2]$ clusters: syntheses, structures, and magnetic properties. *RSC Adv.* **2016**, *6*, 12408−12413.
(18) Chandrasekhar, V.; Bag, P.; Speldrich, M.; van Leusen, J.; Kögerler, P. Synthesis, Structure, and Magnetic Properties of a New Family of Tetra-nuclear {Mn2IIILn2}(Ln = Dy, Gd, Tb, Ho) Clusters With an Arch-Type Topology: Single-Molecule Magnetism Behavior in the Dysprosium and Terbium Analogues. *Inorg. Chem.* **2013**, *52*, 5035−5044.
(19) Ledezma-Gairaud, M.; Grangel, L.; Aromí, G.; Fujisawa, T.; Yamaguchi, A.; Sumiyama, A.; Sañudo, E. C. From Serendipitous Assembly to Controlled Synthesis of 3d−4f Single-Molecule Magnets. *Inorg. Chem.* **2014**, *53*, 5878.
(20) Cao, F.; Wang, S.; Li, D.; Zeng, S.; Niu, M.; Song, Y.; Dou, J. Family of Mixed 3d−4f Dimeric 14-Metallacrown-5 Compounds: Syntheses, Structures, and Magnetic Properties. *Inorg. Chem.* **2013**, *52*, 10747−10755.
(21) Woodruff, D. N.; Winpenny, R. E. P.; Layfield, R. A. Lanthanide Single-Molecule Magnets. *Chem. Rev.* **2013**, *113*, 5110−5148.
(22) Xie, Q. W.; Cui, A. L.; Tao, J.; Kou, H. Z. Syntheses, structure, and magnetic properties of hexanuclear $Mn^{III}_2M^{III}_4$ (M = Y, Gd, Tb, Dy) complexes. *Dalton Trans.* **2012**, *41*, 10589.
(23) Liu, J.; Ma, C.; Chen, H.; Hu, M.; Wen, H.; Cui, H.; Chen, C. The first heterometallic examples of 3d−4f heptanuclear $[Mn^{II}_3Ln^{III}_4]$ complexes with planar disc-like cores and diverse magnetic properties. *Dalton Trans.* **2013**, *42*, 3787−3790.
(24) Langley, S. K.; Moubaraki, B.; Murray, K. S. A heptadecanuclear $Mn^{III}_9Dy^{III}_8$ cluster derived from triethanolamine with two edge sharing supertetrahedra as the core and displaying SMM behavior,. *Dalton Trans.* **2010**, *39*, 5066−5069.
(25) Li, M.; Lan, Y.; Ako, A. M.; Wernsdorfer, W.; Anson, C. E.; Buth, G.; Powell, A. K.; Wang, Z.; Gao, S. A family of 3d-4f octanuclear Mn(III)(4)Ln(III)(4) wheels (Ln = Sm, Gd, Tb, Dy, Ho, Er, and Y): synthesis, structure, and magnetism. *Inorg. Chem.* **2010**, *49*, 11587−11594.
(26) Moreno Pineda, E.; Chilton, N. F.; Tuna, F.; Winpenny, R. E. P.; McInnes, E. J. L. Systematic Study of a Family of Butterfly-Like {M2Ln2} Molecular Magnets (M = Mg(II), Mn(III), Co(II), Ni(II), and Cu(II); Ln = Y(III), Gd(III), Tb(III), Dy(III), Ho(III), and Er(III)). *Inorg. Chem.* **2015**, *54*, 5930−5941.
(27) Ako, A. M.; Mereacre, V.; Clérac, R.; Wernsdorfer, W.; Hewitt, I. J.; Anson, C. E.; Powell, A. K. A $[Mn_{18}Dy]$ SMM resulting from the targeted replacement of the central Mn^{II} in the S = 83/2 $[Mn_{19}]$-aggregate with Dy^{III}. *Chem. Commun.* **2009**, 544−546.
(28) Vallejo, J.; Pascual-Álvarez, A.; Cano, J.; Castro, I.; Julve, M.; Lloret, F.; Krzystek, J.; De Munno, G.; Armentano, D.; Wernsdorfer, W.; Ruiz-García, R.; Pardo, E. Field-induced hysteresis and quantum tunneling of the magnetization in a mononuclear manganese(III) complex. *Angew. Chem., Int. Ed.* **2013**, *52*, 14075−14079.
(29) Lin, S.-Y.; Wang, C.; Zhao, L.; Wu, J.; Tang, J. Chiral mononuclear lanthanide complexes and the field-induced single-ion magnet behaviour of a Dy analogue. *Dalton Trans.* **2015**, *44*, 223−229.
(30) Liu, J.-L.; Yuan, K.; Leng, J.-D.; Ungur, L.; Wernsdorfer, W.; Guo, F.-S.; Chibotaru, L. F.; Tong, M.-L. A six-coordinate ytterbium complex exhibiting easy-plane anisotropy and field-induced single-ion magnet behavior. *Inorg. Chem.* **2012**, *51*, 8538−8544.
(31) Grigoropoulos, A.; Pissas, M.; Papatolis, P.; Psycharis, V.; Kyritsis, P.; Sanakis, Y. Spin-relaxation properties of a high-spin mononuclear $Mn(III)O_6$-containing complex. *Inorg. Chem.* **2013**, *52*, 12869−12871.
(32) Craig, G. A.; Marbey, J. J.; Hill, S.; Roubeau, O.; Parsons, S.; Murrie, M. Field-Induced Slow Relaxation in a Monometallic Manganese(III) Single-Molecule Magnet. *Inorg. Chem.* **2015**, *54*, 13−15.
(33) Pascual-Álvarez, A.; Vallejo, J.; Pardo, E.; Julve, M.; Lloret, F.; Krzystek, J.; Armentano, D.; Wernsdorfer, W.; Cano, J. Cano, Field-

DOI: 10.1021/acs.inorgchem.7b02575
Inorg. Chem. 2018, 57, 326−334

Induced Slow Magnetic Relaxation in a Mononuclear Manganese-(III)−Porphyrin Complex. *Chem. - Eur. J.* **2015**, *21*, 17299−17307.
(34) Ishikawa, R.; Miyamoto, R.; Nojiri, H.; Breedlove, B. K.; Yamashita, M. Slow relaxation of the magnetization of an Mn(III) single ion. *Inorg. Chem.* **2013**, *52*, 8300−8302.
(35) Chen, L.; Wang, J.; Liu, Y.-Z.; Song, Y.; Chen, X.-T.; Zhang, Y.-Q.; Xue, Z.-L. Slow Magnetic Relaxation in Mononuclear Octahedral Manganese(III) Complexes with Dibenzoylmethanide Ligands. *Eur. J. Inorg. Chem.* **2015**, 271−278.
(36) Guedes, G. P.; Soriano, S.; Mercante, L. A.; Speziali, N. L.; Novak, M. A.; Andruh, M.; Vaz, M. G. F. New Synthetic Route toward Heterometallic 3d−3d′ and 3d−4f Single-Molecule Magnets. The First Co^{II}−Mn^{III} Heterometallic Complex. *Inorg. Chem.* **2013**, *52*, 8309−8311.
(37) *APEX2*, v2014.5-0 ed.; Bruker AXS Inc.: Madison, WI, 2007.
(38) *SAINT*, v8.34A ed.; Bruker AXS Inc.: Madison, WI, 2013.
(39) Sheldrick, G. M. *SADABS*; University of Göttingen: Göttingen, Germany, 1996.
(40) *CRYSALIS RED*, 1.171.32.38 ed.; Oxford Diffraction Ltd.: Abingdon, U.K., 2008.
(41) Sheldrick, G. M. A short history of Shelx. *Acta Crystallogr., Sect. A: Found. Crystallogr.* **2008**, *A64*, 112−122.
(42) Farrugia, L. J. *ORTEP*-3 for Windows - a version of *ORTEP*-III with a Graphical User Interface (GUI). *J. Appl. Crystallogr.* **1997**, *30*, 565.
(43) Momma, K.; Izumi, F. *VESTA 3* for three-dimensional visualization of crystal, volumetric and morphology data. *J. Appl. Crystallogr.* **2011**, *44*, 1272−1276.
(44) Hassan, A. K.; Pardi, L. A.; Krzystek, J.; Sienkiewicz, A.; Goy, P.; Rohrer, M.; Brunel, L. C. Ultrawide Band Multifrequency High-Field EMR Technique: A Methodology for Increasing Spectroscopic Information,. *J. Magn. Reson.* **2000**, *142*, 300−312.
(45) Stoll, S.; Schweiger, A. EasySpin, a comprehensive software package for spectral simulation and analysis in EPR. *J. Magn. Reson.* **2006**, *178*, 42−55.
(46) Takahashi, S.; Hill, S. A rotating cavity for high-field angle-dependent microwave spectroscopy of low-dimensional conductors and magnets,. *Rev. Sci. Instrum.* **2005**, *76*, 023114.
(47) Mola, M.; Hill, S.; Goy, P.; Gross, M Instrumentation for millimeter-wave magnetoelectrodynamic investigations of low-dimensional conductors and superconductors. *Rev. Sci. Instrum.* **2000**, *71*, 186−200.
(48) Hammond, G. S.; Nonhebel, D. C.; Wu, C. H. S. Chelates of *β*-Diketones. V. Preparation and Properties of Chelates Containing Sterieally Hindered Ligands. *Inorg. Chem.* **1963**, *2*, 73−76.
(49) Rinck, J.; Lan, Y.; Anson, C. E.; Powell, A. K. Coordination cluster nuclearity decreases with decreasing rare earth ionic radius in 1:1 Cr/Ln N-butyldiethanolamine compounds: a journey across the lanthanide series from $Cr_4^{(III)}La_4$−$Cr_4^{(III)}Tb_4$ via $Cr_3^{(III)}Dy_3$ and $Cr_3^{(III)}Ho_3$ to $Cr_2^{(III)}Er_2$−$Cr_2^{(III)}Lu_2$. *Inorg. Chem.* **2015**, *54*, 3107−3117.
(50) Llunell, M.; Casanova, D.; Cirera, J.; Alemany, P.; Alvarez, S. *SHAPE: Program for the Stereochemical Analysis of Molecular Fragments by Means of Continuous Shape Measures and Associated Tools*, v2.1; Electronic Structure Group, Univeristat de Bardcelona: Barcelona, Spain, 2013.
(51) Tang, C.; Lu, J.; Han, J.; Liu, Y.; Shen, Y.; Jia, D. Complexations of Ln(III) with SnS_4H and Sn_2S_6: Solvothermal syntheses and characterizations of lanthanide coordination polymers with thiostannate and polyamine mixed ligands. *J. Solid State Chem.* **2015**, *230*, 118−125.
(52) Kang, D.-H.; Ledderboge, F.; Kleinke, H.; Schleid, T. $Pr_3S_2Cl_2[AsS_3]$: A Praseodymium(III) Sulfide Chloride Thioarsenate-(III) with Double Chains of Condensed $[SPr_4]^{10+}$ Tetrahedra. *Z. Anorg. Allg. Chem.* **2015**, *641*, 322−326.
(53) Andruh, M.; Bakalbassis, E.; Kahn, O.; Trombe, J. C.; Porcher, P. Structure and Spectroscopic and Magnetic Properties of Rare Earth Metal(III) Derivatives with the 2-Formyl-4-methyl-6-(N-(2-pyridylethy1)formimidoyl)phenol Ligand. *Inorg. Chem.* **1993**, *32*, 1616−1622.
(54) Pasatoiu, T. D.; Tiseanu, C.; Madalan, A. M.; Jurca, B.; Duhayon, C.; Sutter, J. P.; Andruh, M. Study of the Luminescent and Magnetic Properties of a Series of Heterobinuclear $[Zn^{II}Ln^{III}]$ Complexes. *Inorg. Chem.* **2011**, *50*, 5879−5889.
(55) Azuah, R. T.; Kneller, L. R.; Qiu, Y.; Tregenna-Piggott, P. L. W.; Brown, C. M.; Copley, J. R. D.; Dimeo, R. M. DAVE: A Comprehensive Software Suite for the Reduction, Visualization, and Analysis of Low Energy Neutron Spectroscopic Data. *J. Res. Natl. Inst. Stand. Technol.* **2009**, *114*, 341−358.
(56) Pointillart, F.; Bernot, K. Determination of the Nature of Exchange Interactions in the 3d−4f Magnetic Chain $\{[Cu(salen)Pr(hfac)_3]_2(L)\}_n$ (L = 4,4'-Bipyridine, Pyrazine). *Eur. J. Inorg. Chem.* **2010**, 952−964.
(57) Kahn, O. *Molecular Magnetism*; VCH Publishers, Inc.: New York, 1993.
(58) Krzystek, J.; Telser, J.; Pardi, L. A.; Goldberg, D. P.; Hoffman, B. M.; Brunel, L.-C. High-Frequency and -Field Electron Paramagnetic Resonance of High-Spin Manganese(III) in Porphyrinic Complexes. *Inorg. Chem.* **1999**, *38*, 6121−6129.
(59) Mantel, C.; Chen, H.; Crabtree, R. H.; Brudvig, G. W.; Pecaut, J.; Collomb, M.-N. l.; Duboc, C. High-Spin Chloro Mononuclear Mn^{III} Complexes: A Multifrequency High-Field EPR Study. *ChemPhysChem* **2005**, *6*, 541−546.
(60) Cole, K. S.; Cole, R. H. Dispersion and Absorption in Dielectrics 1. Alternating Current Characteristics. *J. Chem. Phys.* **1941**, *9*, 341.
(61) Costes, M.; Broto, J. M.; Raquet, B.; Rakoto, H.; Novak, M. A.; Sinnecker, J. P.; Soriano, S.; Folly, W. S. D.; Maignan, A.; Hardy, V. J. Dynamic effects in one-dimensional $A_3'ABO_6$. *J. Magn. Magn. Mater.* **2005**, *294*, e123−e126.

DOI: 10.1021/acs.inorgchem.7b02575
Inorg. Chem. 2018, 57, 326−334